Materials Chemistry and Physics 292 (2022) 126858

Contents lists available at ScienceDirect

Materials Chemistry and Physics

journal homepage: www.elsevier.com/locate/matchemphys

Formation of Sn/Zn alloy or core-shell nanoparticles via pulsed nanosecond discharges in liquid toluene

Marta Agati [a,**,1], Ahmad Hamdan [b,*], Simona Boninelli [a,1]

[a] Consiglio Nazionale Delle Ricerche - Istituto per La Microelettronica e i Microsistemi (CNR-IMM), Strada VIII n.5, 95121, Catania, Italy
[b] Groupe de Physique des Plasmas, Département de Physique, Université de Montréal, 1375 Avenue Thérèse-Lavoie-Roux, Montréal, QC, H2V 0B3, Canada

HIGHLIGHTS

- Pulsed nanosecond discharge in liquid toluene produces nanoparticles.
- Three size distributions of nanoparticles are identified.
- Particles with diameter <10 nm are made of Sn–Zn alloy.
- Particles with diameter 10–20 nm are made of Sn-core and Zn-shell.
- Particles with diameter >100 nm are made of Sn.

GRAPHICAL ABSTRACT

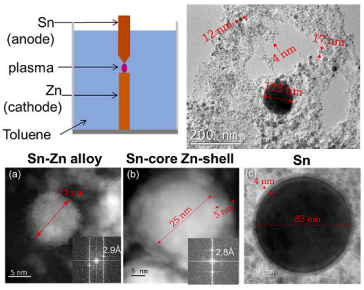

ARTICLE INFO

Keywords:
Electrical discharges
Plasma in liquid
Sn–Zn nanoalloy
Transmission electron microscopy

ABSTRACT

In the exploration of new techniques for the synthesis of metallic nanoparticles, the possibility to exploit electrical discharges in liquid has arisen as an easy, high throughput and low-cost method. This technique of synthesis offers an extensive playground to produce a wide range of nanostructures with composition highly dependent on that of the electrode and of the liquid medium. Here, we demonstrate the formation of a Sn–Zn nanoalloy (particle diameter <10 nm) using electrical discharge between a Sn anode and a Zn cathode immersed in liquid toluene. Core/shell nanoparticles, with diameter between 12 and 20 nm, are also produced. These particles are composed of a Sn crystalline core and a shell made of Zn, Sn and O. A third class of particles was also found, although being rarer, constituted of large (hundreds of nm) Sn particles, with a thin Sn oxide shell. Detailed structural and chemical characterizations were accomplished via TEM and STEM imaging, as well as STEM-EDX analyses on the single nanoparticles and, considering the complex variety of phenomena taking place in in-liquid plasma, a plausible mechanism of synthesis is proposed.

1. Introduction

Because of size reduction and quantum confinement, nanomaterials exhibit enhanced and novel properties as compared to bulk materials [1]. The employment of nanomaterials in smart applications has been advancing and spreading over the most diverse fields, from functional

* Corresponding author.
** Corresponding author.
E-mail addresses: marta.agati@imec.be (M. Agati), ahmad.hamdan@umontreal.ca (A. Hamdan).
[1] Current affiliation: Interuniversity Microelectronics Centre (Imec), Kapeldreef 75, 3001 Leuven, Belgium.

https://doi.org/10.1016/j.matchemphys.2022.126858
Received 30 May 2022; Received in revised form 3 October 2022; Accepted 3 October 2022
Available online 8 October 2022

devices (e.g. energy or data storage [2,3]), to pharmaceuticals (e.g. drug delivery [4]) and catalysts (e.g. production of ammonia [5]), till to aerospace applications (e.g. nanocomposites [6]) and metamaterials (e.g. energy harvesting [7]). Sustaining and further boosting the exploitation of nanomaterials in the market requires the development of high throughput, non-expensive and ecological techniques for their fabrication.

In this panorama, the exploitation of electrical discharges between two metallic electrodes immersed in liquid media has arisen as an extremely easy method to produce large quantities of nanomaterials (yield of ~mg/min) via the erosion of the electrodes and the dissociation of the liquid [8]. In-liquid discharge generates plasma under the conditions of high pressure (tens to hundreds of bars) and temperature (few thousands of Kelvins) [9], which favors the rapid formation of materials at the nanoscale. Different electrodes can be used to enlarge the possible compositions of nanomaterials, e.g. Al. Cu, Ni, Co, etc. [10–13]. Moreover, the possibility to employ different liquid environments alters the final product. For instance, discharges in water often produced metal oxides [11,12], whereas discharges in hydrocarbons often produced nanocomposite materials, i.e. metal nanoparticles embedded in a carbonaceous matrix or shell [14]. Discharges in cryogenic liquid, e.g. liquid nitrogen, have been performed, and metal nanostructures have been produced [15,16]; the production of novel materials via discharges in liquid nitrogen has been also reported [17].

Clearly, the research on this topic offers an extensive playground for the investigation of the obtained nanomaterials' structural and chemical properties. From a fundamental point of view, the full understanding of the synthesis process calls for a comprehensive description of the in-liquid discharge. Despite the highly facile setup to induce discharges in liquid (i.e. two metallic electrodes immersed in liquid), it does not exist a univocal theory explaining neither the physical and chemical mechanisms of the discharge nor the growth of nanostructures [18]. To finely control the desired product by in-liquid discharge, the main challenge is the control of this unconventional and out-of-equilibrium thermodynamical plasma. For example, it has been difficult to obtain metallic nano-alloys by simply combining two different electrodes [15,16,19–21]. More often, the synthesis of nano-alloys relies on the use of sintered electrodes: in this case, the metallic elements simultaneously present in the electrodes are found in the form of nano-alloys, having compositions depleted of the more volatile element [16]. Also, nano-alloys have been synthesized via a two-step procedure [19]. For example, in the case of Co_xNi_{1-x} alloy nanoparticles, Ni nanoparticles are synthesized first, using electrical discharges between two Ni electrodes in liquid nitrogen; then, the obtained colloid is used as a medium for the discharge between two Co electrodes. Hence, it is important to investigate in more depth the possibility to synthesize nano-alloys via electrical discharges in liquid in a single-step process and to understand their formation mechanism.

In this framework, we demonstrate that pulsed discharges in liquid toluene between Sn anode and Zn cathode produce Sn–Zn metallic alloy, as well as other structures. Sn-based nanomaterials have showed great properties, particularly in the field of microwave communication, as they are considered excellent absorbers of frequencies in the range of 2–18 GHz [22–24]. The structural and chemical characteristics of the produced nanomaterial were studied via Transmission Electron Microscopy (TEM). The compositional analyses performed by Energy Dispersive X-Ray Spectroscopy (EDX) were of paramount importance to analyze the different chemical compositions of the nanoparticles and to assess the formation of the metallic Sn–Zn alloy. Finally, we propose the growth mechanism underlying the nanostructure formation and the generation of the Sn–Zn nano-alloy. These results open the way towards a major comprehension of nano-alloy formation via electrical discharges in liquid media.

2. Experimental setup and characterization techniques

The experimental setup used to synthesize Sn and Zn nanoparticles as well as the Sn–Zn nano-alloy is depicted in Fig. 1(a). We employed a cylindrical quartz cell (inner and outer diameters of 2.4 and 2.6 cm, respectively) filled with 15 mL of toluene. We performed the synthesis process employing Sn anode and Zn cathode (from GoodFellow, purity of 99.99%). The electrodes consisted of rods with diameter of 2 mm. The head of the anode was polished to have sharp tip (curvature radius of ~20 μm), and the cathode surface was flat. The initial interelectrode distance was ~50 μm and was adjusted during experiments to compensate electrode erosion. The adjustment was based on the breakdown moment in the pulse by keeping it almost at the same time. The electrical discharges are generated via a nanosecond positive pulsed power supply (NSP 120-20-P-500-TG-H, Eagle Harbor Technologies), which delivered 5 kV of voltage amplitude and 500 ns of pulse width. The electrical characteristics (voltage and current) of the discharge were measured by using a high-voltage probe (P6015A, Tektronix) and a current monitor (6585, Pearson), while the corresponding waveforms are visualized and recorded by using an oscilloscope (MSO54, 2 GHz, 6.25 GS/s); current-voltage waveforms for a typical discharge are shown in Fig. 1(b). The behavior of the waveforms (voltage drop and current peak followed by oscillations) indicates that the discharge is running in spark mode. The discharge repetition rate was 10 Hz, and the total duration of an experiment was 10 min. Based on the electrode erosion (quantified using optical microscope), the quantity of material synthesized under the present conditions is ~15 μg.

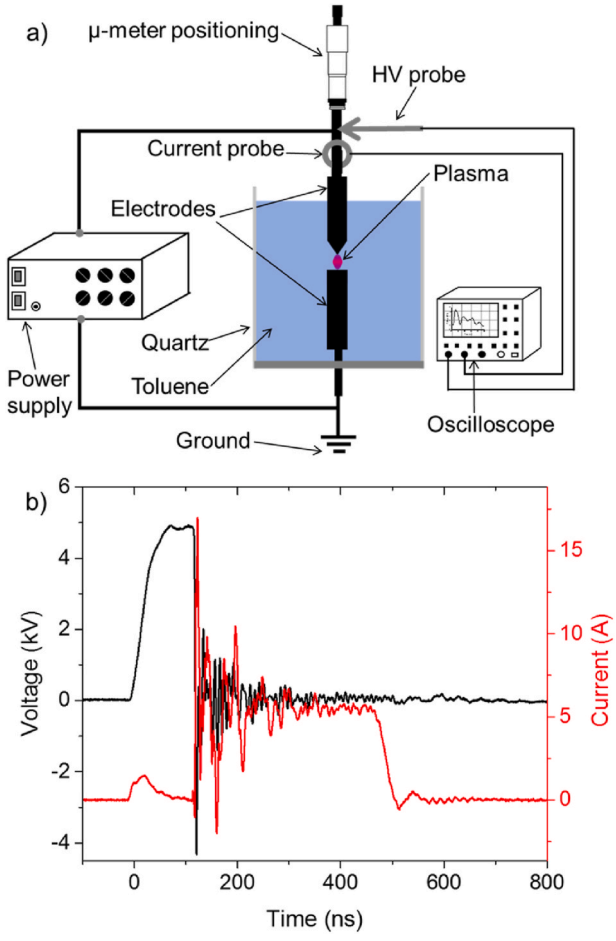

Fig. 1. a) Experimental setup employed for the synthesis of Sn–Zn nanoparticles via pulsed electrical discharges in toluene and b) current-voltage characteristics for a typical discharge.

The samples (liquid containing the nanoparticles) obtained by the discharges under the abovementioned conditions were sonicated for 10 min and drop-casted on TEM Cu or Au C-lacey grids. We chose not to use grids endowed with an underlying continuous C-films to perform reliable chemical analyses on these C-containing nanomaterials. To investigate the morphology of the nanomaterials, we performed bright field TEM (BF-TEM) imaging, using a Jeol JEM 2010F microscope with electron beam energy set at 200 keV. More detailed structural analyses were performed via scanning transmission electron microscopy (STEM) in both bright field (BF-STEM) and high angle annular dark field (HAADF-STEM) modes. Compositional analyses were performed by employing STEM-EDX in spectrum imaging (SI) mode, which is an extremely powerful technique that carries out the spectroscopic information pixel-per-pixel. In this technique, single EDX spectra are acquired during the STEM imaging acquisition pixel-by-pixel, hence allowing to correlate the spatial information with the chemical composition in one single pixel. EDX spectra can be integrated over the nanoparticle or including the region around it, as done in the paper. In this way, it is possible to obtain one single EDX spectrum carrying not only the quantitative information of the chemical elements composing the sample, but also their spatial distribution. The quantification is based on background subtraction via the Kramers correction mode and the Casnati cross-section model. Moreover, as long as each element is identified via its EDX peaks in the spectrum, the analysis of each spectrum pixel-by-pixel can provide the quantitative distribution of the chemical element via color intensity, hence allowing to obtain the spatial map of the element.

STEM analyses were carried out by using a Jeol ARM 200F microscope (at 200 keV) equipped with probe aberration corrector to perform high resolution imaging. This microscope is also equipped with a 100-mm^2 silicon drift detector to perform EDX analyses.

3. Results

Fig. 2 reports large view BF-TEM images of the nanomaterial obtained by discharges between electrodes made of Sn and Zn at different magnifications. These images show the global morphological characteristics of the nanoparticles and clearly indicate that they have different sizes (from few to hundreds of nanometers) and spherical geometry.

By performing several morphological analyses in more detail, we identified three main groups of nanoparticles:

(i) the majority of the synthesized material is constituted by ultra-small particles, with diameter of few nm (4–6 nm), in general <12 nm, embedded in an amorphous matrix.
(ii) Some nanoparticles have diameters of few tens of nm, ranging between 12 and 20 nm; although the presence of a C matrix surrounding these nanoparticles cannot be obviously deducted from Fig. 2, this aspect can be better understood after performing chemical analyses, as discussed in the following part of the paper.
(iii) The third category is given by larger nanoparticles, having diameter >80 nm and, in general, of the order of few hundreds of nm.

The smallest nanoparticles, belonging to the first group, represent the main product of the nanoparticles synthesized with our technique, while the nanoparticles belonging to the second group can be estimated to be 1/1000. The largest ones, belonging to group 3, can be considered as a by-product since their presence is quite rare in the sample and can be accounted to be less than 1/500000. Complementary measurements using other techniques, such as dynamic light scattering, will be useful to further confirm the size distributions.

The first family of nanoparticles is better illustrated by HAADF-STEM images at atomic resolution, as shown in Fig. 3(a). The homogenous contrast and the presence of lattice fringes inside the nanoparticle indicates the presence of a single-phase monocrystalline arrangement with an interplanar distance equal to 2.9 Å, as evaluated by the corresponding Fast Fourier Transform showed in the inset. This result is confirmed by the analysis of tens of nanoparticles belonging to this first group. The second family of nanostructures, as observed by HAADF-STEM imaging in Fig. 3(b), exhibits a core-shell structure. The lattice fringes are present only in the core of the nanoparticle (having diameter of 25 nm), while the surrounding shell does not have them, indicating that the core is crystalline while the shell is amorphous. The corresponding FFT is also given in the inset (giving interplanar distance of (2.8 Å). The particle with largest diameter, belonging to the third category, is shown in the BF-TEM image reported in Fig. 3(c); these particles also exhibit core-shell structure, and the showed one has a core with diameter of ~83 nm and a shell thickness of ~4 nm.

As a further step of our investigations, we studied the compositional properties of all these nanostructures by using the SI method. The chemical maps can be extracted afterwards from the SI data set. First, we focused on the first family of nanostructures, i.e. the smallest ones.

Fig. 4(a) shows a HAADF-STEM image of nanoparticles belonging to the first group. EDX spectrum shown in Fig. 4(b) is extracted from the region indicated by the blue square in Fig. 4(a). Clearly, this

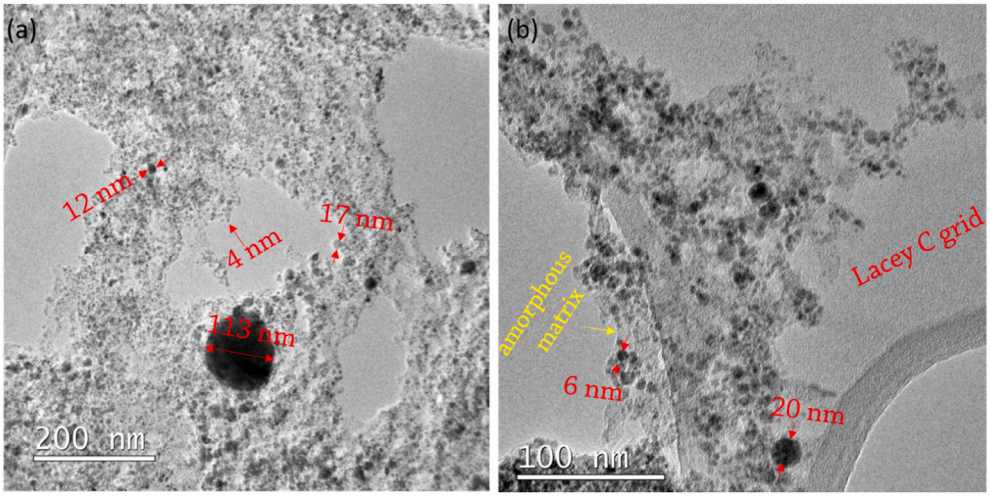

Fig. 2. BF-TEM images at different magnifications, showing the overall morphological characteristics of the nanomaterials obtained by discharges between Sn and Zn electrodes in liquid toluene.

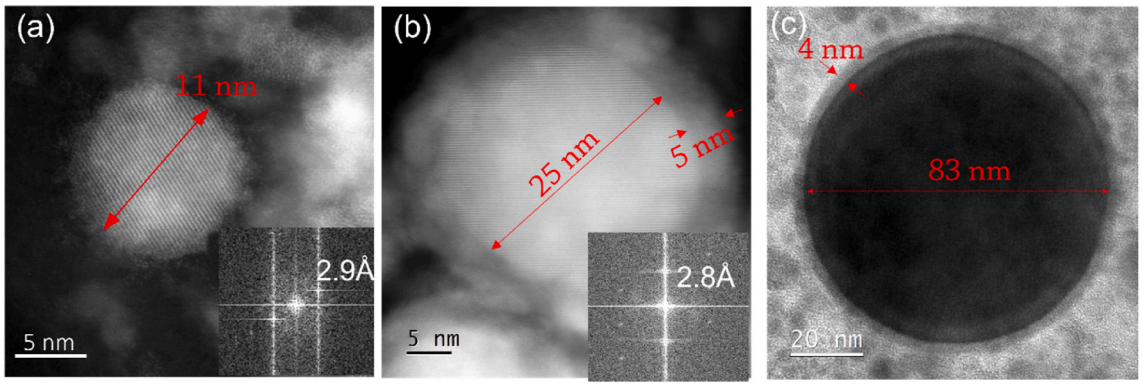

Fig. 3. HAADF-STEM (a,b) and BF-TEM (c) images showing the three families of nanoparticles.

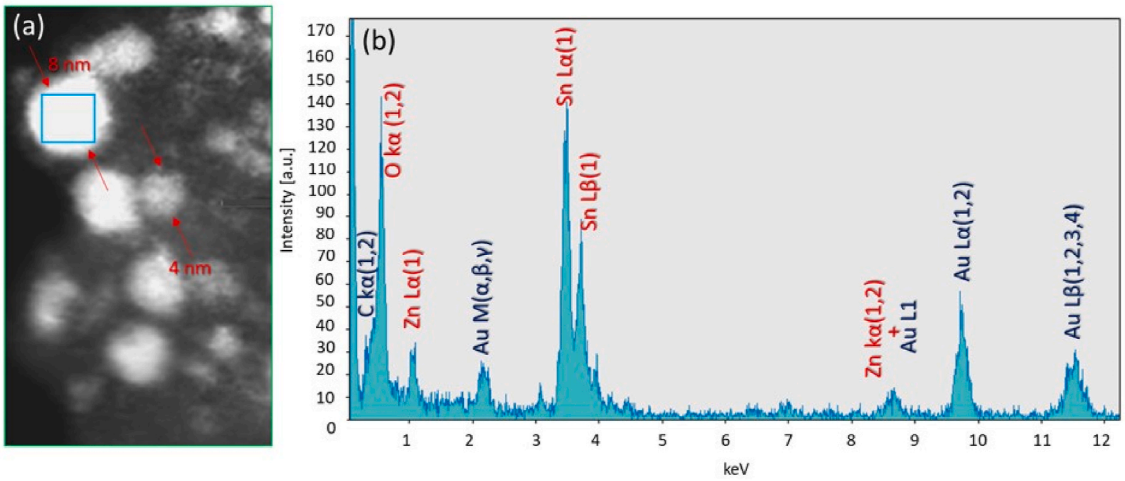

Fig. 4. (a) HAADF-STEM image showing some nanoparticles belonging to the first group (their sizes do not exceed 8 nm of diameter) (b) EDX spectrum extracted from one nanoparticle, from the region represented by the blue square. (For interpretation of the references to color in this figure legend, the reader is referred to the Web version of this article.)

nanoparticle contains both Sn and Zn, as well as O. Au signal is due to the supporting TEM grid. The C peak can be distinguished as a shoulder of the O signal, since these two peaks are very close in energy. The spatial distribution of the chemical elements in the region of interest can be clarified thanks to the EDX maps, as shown in Fig. 5. Fig. 5(a) displays the raw maps relatively to the different elements revealed in the EDX spectrum. Most interestingly, we can observe that Sn and Zn signals are homogeneously present in the nanoparticles, as. it is better evidenced by the quantitative line profile reported in Fig. 5(b). We can also see that the C distribution corresponds very well to the amorphous matrix which envelops the nanomaterials and originates from the toluene decomposition by the discharge. Similar results were obtained performing EDX analyses on nanoparticles belonging to the first group.

Quantitative EDX analysis of the nanoparticle indicated in Fig. 5 led us to conclude that this nanoparticle averagely contains Sn 61%, Zn 17%, O 22%. Similar analyses were performed on different nanoparticles with diameter <10 nm and demonstrated that these nanoparticles have the characteristics of the Sn–Zn alloy, having contents of Sn and Zn varying in the range of 52–67% of Sn and 9–25% of Zn. O most likely arises from the oxidation of these nanoparticles after air-exposure (this claim will be further supported in the Discussion).

Chemical characterizations were performed also on the second group of nanoparticles, represented by core-shell nanoparticles having diameter of few tens of nm, as summarized in Fig. 6. The crystalline nature of the core is also evident in the enlarged image of the region of interest, reported as inset of Fig. 6(a). The quantitative line profile across the selected nanoparticle is reported in Fig. 6(b), while the corresponding EDX elemental maps are illustrated in Fig. 6(c). From the analysis of numerous nanoparticles of the same type, we inferred that the nanoparticle core is mostly composed by crystalline Sn, while the shell is a mixture of Sn and Zn. The oxygen is mostly present in the outer shell of the nanoparticle and is due to the oxidation of the nanoparticles during air exposure. Moreover, we can see that the C map presents a darker spherical shadow corresponding to the nanoparticle showed in 6(a) with Sn core and Zn–Sn–O shell, indicating that also this group of nanoparticles is surrounded by a C matrix.

Finally, we perform chemical analyses of the large particles belonging to the third category of nanostructures found in this sample. In this case, we found that the Zn is almost absent, and the nanoparticle is mainly composed of Sn with a Sn oxide shell. EDX maps for a typical particle are shown in Fig. 7.

4. Discussion

It has been often found that the synthesis of nanoparticles with nanosecond electrical discharges in liquid led to the formation of nanoparticles with different size distributions within the same sample. The presence of different families of nanostructures indicates that more than one formation mechanism take place simultaneously during the synthesis process. Similar to those found in our samples, three distributions of nanoparticles are usually reported for material synthesized during discharges, although different liquid (including water, liquid

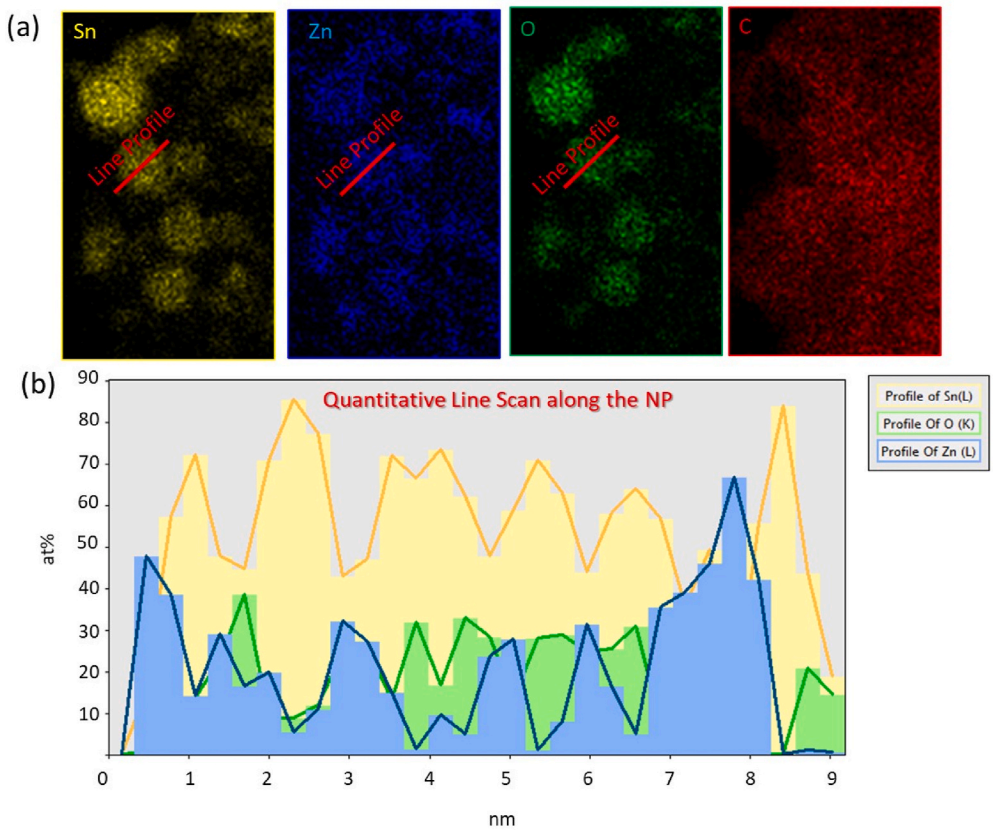

Fig. 5. Results of the chemical analysis of nanoparticles belonging to the first group, as reported in Fig. 4. (a) EDX maps displaying the spatial distribution of the chemical elements composing the nanoparticle. (b) Quantitative line scan across the nanoparticle.

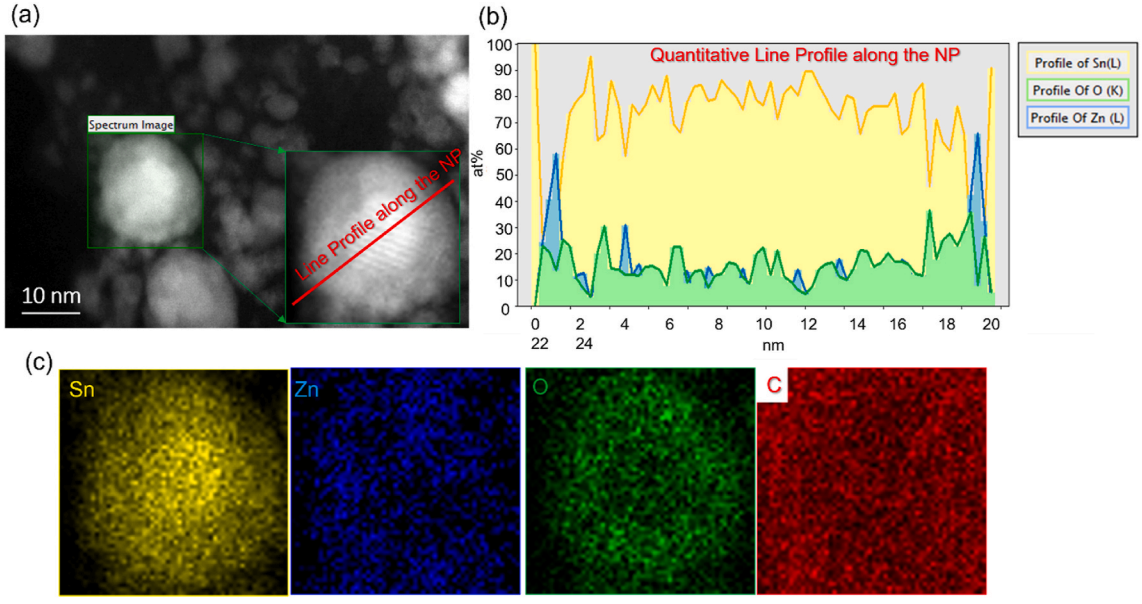

Fig. 6. (a) HAADF-STEM image showing a core/shell nanoparticle having diameter of 18 nm and representing the second group of nanoparticles present in this sample. (b) Quantitative line scan across the nanoparticle (c) EDX maps displaying the spatial distribution of the chemical elements composing the nanoparticle.

hydrocarbon or liquid nitrogen) or electrodes (including Al, Pt, Cu, Ni, Co, etc.) were utilized [10,12,19,25]. Currently, at least for electrodes with same chemical composition, it is well accepted that the larger particles have been ascribed to the ejection of liquid droplets from the electrode surfaces struck by the discharge, while the occurrence of the smaller nanoparticles (<10 nm) has been explained in terms of phase condensation in the plasma core; the particles of tens of nm are related to phase condensation in the plasma edge. Optical emission spectroscopy has been performed on discharges in various conditions [10,19,25], and it is well accepted that atoms will be evaporated from electrode surface and injected in the plasma where they are excited and ionized. Due to the high pressure and temperature in the discharge, agglomeration can

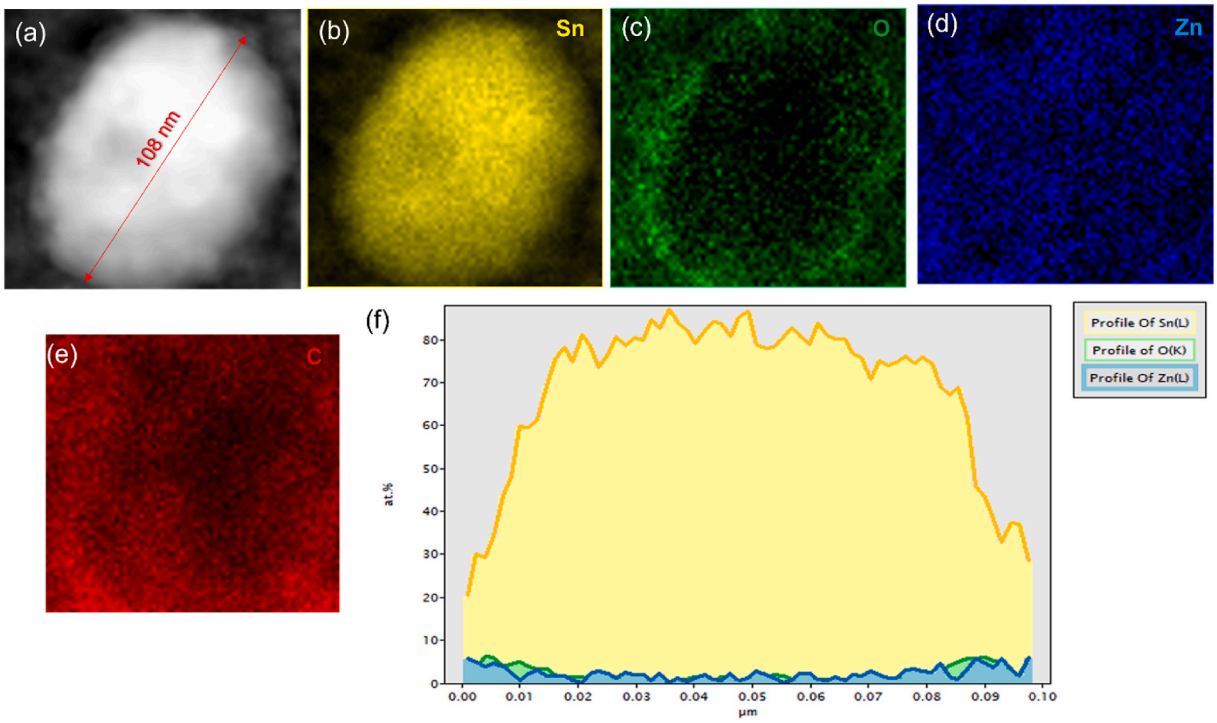

Fig. 7. (a) HAADF-STEM image of a large nanoparticle having diameter of more than 100 nm, hence belonging to the third group of nanoparticles forming our sample. (b–e) EDX maps displaying the spatial distribution of the chemical elements composing this nanoparticle. (f) Quantitative line scan across the nanoparticle.

happen and nanoparticles are produced. This description remains basic, there are many other factors that should be considered, in particular the action of shock waves and bubble dynamics (i.e. pressure dynamics) on the products. In the case of electrodes with different chemical composition, the mechanisms of synthesis seem to be different. Although such experiments were performed in the aim to produce nanoalloys, these latter were produced only in specific conditions. For instance, discharge between Cu–Zn alloyed electrodes in liquid nitrogen did not produce nanoalloys, but rather core-shell nanoparticles [15]. Similar results were obtained when two-steps discharges (first with Cu electrodes then with Zn electrodes in the liquid previously enriched with Cu nanoparticles) are conducted in liquid nitrogen [26]. On the other hand, Trad et al. [19] have conducted discharges in liquid nitrogen with Co and Ni electrodes, and they showed the possibility to produce Co–Ni nanoalloys. The authors attributed the feasibility to a sufficiently long residence time of both Ni and Co clusters within the discharge and to their total miscibility.

In our conditions, the nature of the produced nanoparticles is size dependent. Indeed, the smallest ones (<10 nm) are made of Sn–Zn nanoalloy, those measuring tens of nm are made of Sn core and Zn shell, and the largest ones (hundreds of nm) are made of Sn (with an oxidized shell). Fig. 8 shows a descriptive scenario of synthesis (all phenomena are added in Figure (8)b, and individual ones are depicted in Fig. 8(c–e). It is well accepted that the largest particles are due to ejection of molten material from the electrode. In general, the plasma starts propagating from the sharp electrode, i.e. Sn electrode, then it reaches the Zn cathode within only few of nanoseconds. The fact that the detected large particles were made of Sn (not large Zn particles were detected) can be explained by two facts: i) the difference in melting temperature of both material (505 K for Sn and 693 for Zn) and ii) the sharp Sn anode tip, which means a relatively high current density (i.e. high temperature). In this context, the tip of the anode Sn will be heated and melted first, and molten material could be ejected (i.e. Fig. 8(c)). For the same reason, it is expected that Sn atoms will evaporate before Zn atoms. At this step, evaporated Sn atoms can follow two ways: i) on-axis propagation (i.e. in the plasma core) or ii) off-axis propagation (i.e. in the plasma edge). Sn atoms following way (i) will reach relatively quickly evaporated Zn atoms. Then, as described by Trad et al. [19] concerning the formation of Co–Ni nano-alloys, a vapor mixture of both Sn and Zn forms clusters. During the residence time of these clusters in the plasma phase, the repetitive collisions between them favor the mixing of the two elements to form the nanoalloy (Fig. 8(d)). This may explain the formation mechanism of Sn–Zn nanoalloys with diameter <10 nm.

The remaining distribution, particles with 10s of nm diameter, made

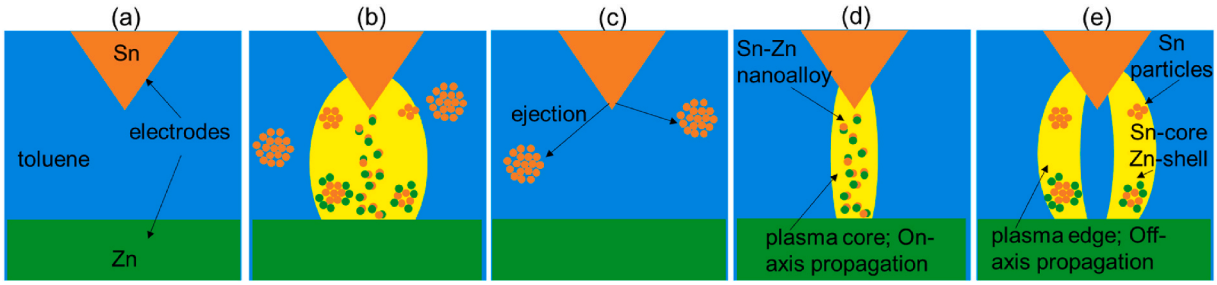

Fig. 8. Schematic of the different phenomena taking place during electrical discharges in toluene, giving rise to the three families of nanostructures described in the paper.

of Sn core and Zn shell, may be explained by the evaporated Sn atoms that propagate off-axis in the plasma edge (way ii); the origin of this propagation can be either the emission of shock wave (i.e. confinement in an iso-pressure plane) or the divergent pin-to-plate geometry. Naturally, it is expected that Sn atoms will agglomerate to form Sn nanoparticles before reaching Zn atoms/clusters. At this moment, the latter will aggregate/agglomerate with Sn nanoparticles, resulting thus in core-shell Sn–Zn nanoparticles (Fig. 8(e)).

As for the oxidation processes in plasma phase or, later, in the liquid are not likely to occur because the lack of oxidative species, although water impurities or dissolved air can be present. Therefore, we believe that the oxidation of nanoparticles is due to air exposure after the evaporation of toluene prior to the characterization of the sample. Hence, depending on the initial size of the nanoparticles, oxidation may result in their full oxidation, which is the case for the nanoparticles with sizes <10 nm, and in core/shell metal/metal-oxide nanoparticles for particles with larger sizes [10].

5. Conclusions

This paper reported the synthesis of nanostructures via pulsed electrical discharges in liquid toluene, by employing a Sn anode and a Zn cathode. As a result, three main families of nanostructures are identified: (i) ultra-small particles, with diameter of few nm (4–6 nm), in general <12 nm, embedded in an amorphous matrix; (ii) some nanoparticles have diameters of few tens of nm, ranging between 12 and 20 nm; (iii) the third category is given by larger nanoparticles, having diameter >80 nm and, in general, of the order of few hundreds of nm. The first family constitutes the majority of the synthesized material and, as demonstrated by chemical analyses on the single nanoparticles, exhibits the characteristics of a Sn–Zn nanoalloy, which gets oxidized after air exposure. The second group of nanoparticles are core/shell and have a Sn crystalline core, while the shell contains Sn, Zn as well as some O. The third category (very rare) consists of Sn particles with a thin Sn oxide shell. Based on the characteristics of in-liquid discharges, a scenario of growth mechanism was proposed. The first group of smallest Sn–Zn nanoparticles are generated by on-axis propagation of the Sn and Zn atoms in the plasma which, after collision in the vapor mixture, are favored to form nanoalloy compounds. The second group of nanoparticles may be explained by off-axis evaporation of the Sn atoms, agglomerating before reaching Zn atoms, which are thus aggregated later in the shell of the already formed Sn nanoparticles. Finally, the largest particles are due to ejection of molten material from the sharp electrode i.e., the Sn anode, which has also lower melting temperature than Zn.

CRediT authorship contribution statement

Marta Agati: TEM characterizations, Formal analysis, Writing – review & editing. **Ahmad Hamdan:** Conceptualization, Methodology, Writing – review & editing. **Simona Boninelli:** Writing – review & editing.

Declaration of competing interest

The authors declare that they have no known competing financial interests or personal relationships that could have appeared to influence the work reported in this paper.

Data availability

Data will be made available on request.

Acknowledgements

This project has received funding from the European Union's Horizon 2020 research and innovation program under grant agreement No 823717 – ESTEEM3.

References

[1] E. Roduner, Chem. Soc. Rev. 35 (7) (2006) 583–592.
[2] Q. Zhang, E. Uchaker, S.L. Candelaria, G. Cao, Chem. Soc. Rev. 42 (7) (2013) 3127–3171.
[3] M. Gu, Q. Zhang, S. Lamon, Nat. Rev. Mater. 1 (12) (2016) 1–14.
[4] P. Couvreur, Adv. Drug Deliv. Rev. 65 (1) (2013) 21–23.
[5] *Nanoparticle catalysis for ammonia production.
[6] A. Bhat, S. Budholiya, S.A. Raj, M.T.H. Sultan, D. Hui, A.U.M. Shah, S.N.A. Safri, Nanotechnol. Rev. 10 (1) (2021) 237–253.
[7] Z. Chen, B. Guo, Y. Yang, C. Cheng, Phys. B Condens. Matter 438 (2014) 1–8.
[8] N. Sano, H. Wang, M. Chhowalla, I. Alexandrou, G.A.J. Amaratunga, Nature 414 (2001) 506–507.
[9] A. Hamdan, C. Noel, F. Kosior, G. Henrion, T. Belmonte, J. Acoust. Soc. Am. 134 (2013) 991–1000.
[10] A. Hamdan, C. Noël, J. Ghanbaja, T. Belmonte, Plasma Chem. Plasma Process. 34 (5) (2014) 1101–1114.
[11] A. Hamdan, X. Glad, M.S. Cha, Nanomaterials 10 (2020) 1–13, 1347.
[12] A. Hamdan, M. Agati, S. Boninelli, Plasma Chem. Plasma Process. 41 (1) (2021) 433–445.
[13] T. Merciris, F. Valensi, A. Hamdan, J. Appl. Phys. 129 (2021), 063303, 1-13.
[14] X. Glad, J. Gorry, M.S. Cha, A. Hamdan, Sci. Rep. 11 (2021) 7516.
[15] H. Kabbara, J. Ghanbaja, C. Noël, T. Belmonte, Mater. Chem. Phys. 207 (2018) 350–358.
[16] H. Kabbara, J. Ghanbaja, C. Noël, T. Belmonte, Mater. Chem. Phys. 217 (2018) 371–378.
[17] A. Hamdan, H. Kabbara, C. Noël, J. Ghanbaja, A. Redjaimia, T. Belmonte, Particuology 40 (2018) 152–159.
[18] M. Agati, S. Boninelli, A. Hamdan, Mater. Chem. Phys. 261 (2021), 124244.
[19] M. Trad, A. Nominé, C. Noël, J. Ghanbaja, M. Tabbal, T. Belmonte, Plasma Process. Polym. 17 (5) (2020), 1900255.
[20] H. Kabbara, C. Noël, J. Ghanbaja, K. Hussein, D. Mariotti, V. Švrček, T. Belmonte, Sci. Rep. 5 (2015), 17477.
[21] M. Trad, A. Nominé, N. Tarasenka, J. Ghanbaja, C. Noël, M. Tabbal, T. Belmonte, Front. Chem. Sci. Eng. 13 (2019) 360.
[22] Z.H. Wang, D.Y. Geng, Z. Han, Z.D. Zhang, J. Appl. Phys. 108 (2010), 013903.
[23] Z.H. Wang, Z. Han, D.Y. Geng, Z.D. Zhang, Chem. Phys. Lett. 489 (2010) 187–190.
[24] Z.H. Wang, X. He, X. Wang, Z. Han, D.Y. Geng, Y.L. Zhu, Z.D. Zhang, J. Phys. D Appl. Phys. 43 (2010), 495404.
[25] A. Hamdan, C. Noël, J. Ghanbaja, S. Migot-Choux, T. Belmonte, Mater. Chem. Phys. 142 (2013) 199–206.
[26] H. Kabbara, J. Ghanbaja, C. Noël, T. Belmonte, Nano-Struct. Nano-Objects 10 (2017) 22–29.